

Langmuir Probe Measurements within the Discharge Channel of the 20-kW NASA-300M and NASA-300MS Hall Thrusters

IEPC-2013-122

*Presented at the 33rd International Electric Propulsion Conference,
The George Washington University • Washington, D.C. • USA
October 6 – 10, 2013*

Rohit Shastry¹, Wensheng Huang², Thomas W. Haag³ and Hani Kamhawi⁴
NASA Glenn Research Center, Cleveland, OH, 44135, USA

Abstract: NASA is presently developing a high-power, high-efficiency, long-lifetime Hall thruster for the Solar Electric Propulsion Technology Demonstration Mission. In support of this task, studies have been performed on the 20-kW NASA-300M Hall thruster to aid in the overall design process. The ability to incorporate magnetic shielding into a high-power Hall thruster was also investigated with the NASA-300MS, a modified version of the NASA-300M. The inclusion of magnetic shielding would allow the thruster to push existing state-of-the-art technology in regards to service lifetime, one of the goals of the Technology Demonstration Mission. Langmuir probe measurements were taken within the discharge channels of both thrusters in order to characterize differences at higher power levels, as well as validate ongoing modeling efforts using the axisymmetric code Hall2De. Flush-mounted Langmuir probes were also used within the channel of the NASA-300MS to verify that magnetic shielding was successfully applied. Measurements taken from 300 V, 10 kW to 600 V, 20 kW have shown plasma potentials near anode potential and electron temperatures of 4-12 eV at the walls near the thruster exit plane of the NASA-300MS, verifying magnetic shielding and validating the design process at this power level. Channel centerline measurements on the NASA-300M from 300 V, 10 kW to 500 V, 20 kW show the electron temperature peak at approximately 0.1-0.2 channel lengths upstream of the exit plane, with magnitudes increasing with discharge voltage. The acceleration profiles appear to be centered about the exit plane with a width of approximately 0.3-0.4 channel lengths. Channel centerline measurements on the NASA-300MS were found to be more challenging due to additional probe heating. Ionization and acceleration zones appeared to move downstream on the NASA-300MS compared to the NASA-300M, as expected based on the shift in peak radial magnetic field. Additional measurements or alternative diagnostics will be needed to verify peak electron temperatures in the NASA-300MS and compare them with model predictions.

Nomenclature

C	=	line capacitance
I_{cap}	=	capacitive current
L	=	thruster channel length
\dot{m}_a	=	anode mass flow rate

¹ Research Engineer, Propulsion and Propellants Branch, rohit.shastry@nasa.gov.

² Research Engineer, Propulsion and Propellants Branch, wensheng.huang@nasa.gov.

³ Propulsion Engineer, Space Propulsion Branch, thomas.w.haag@nasa.gov.

⁴ Research Engineer, Propulsion and Propellants Branch, hani-kamhawi-1@nasa.gov.

n_e	=	electron number density
P_d	=	discharge power
T	=	thrust
T_e	=	electron temperature
V_d	=	discharge voltage
V_f	=	probe floating potential
ζ	=	proportionality factor
η_a	=	anode efficiency
ϕ_p	=	plasma potential

I. Introduction

HALL thrusters are an electric propulsion technology that are becoming a more attractive option for NASA human exploration and science missions. Under the Space Technology Mission Directorate (STMD), NASA is presently developing a 10- to 15-kW Hall thruster to support the Solar Electric Propulsion Technology Demonstration Mission (SEP TDM). As part of this effort, a number of measurements were taken on previously developed high-power Hall thrusters, including the NASA-300M and NASA-457Mv2.¹⁻⁵ These measurements were intended to help better understand Hall thruster operation at elevated power levels. In particular, performance, near-field plume, far-field plume, and internal measurements were performed on the 20-kW NASA-300M (hereafter referred to as the 300M). The purpose of the internal measurements is to determine how the plasma inside and just downstream of the channel changes as a function of operating condition at these power levels. This in turn complements the trends seen in the performance and plume data to provide a complete picture of thruster performance and operation. Furthermore, these data can be used to validate ongoing modeling efforts at the Jet Propulsion Laboratory (JPL) on high-power Hall thrusters.⁶

One of the goals for the SEP TDM is to push Hall thruster technology beyond existing state-of-the-art, including service lifetimes into the tens of thousands of hours. In order to accomplish this, the concept of magnetic shielding would be incorporated into the design. This concept was initially explained by JPL as the reason behind the near-zero erosion rates observed in the BPT-4000 Qualification Life Test (QLT) after ~5,600 hours.⁷ Since then they have performed a significant amount of work demonstrating the concept and investigating how thruster operation changes with magnetic shielding on a 6-kW laboratory thruster.⁸⁻¹⁰ While the reader is encouraged to read the previous references to fully understand magnetic shielding, the concept will be briefly discussed here.

Since electron conductivity is very high along a magnetic field line compared to across them, electrons can quickly equilibrate along a magnetic field line. In other words, magnetic field lines can be considered isothermal. The same type of reasoning can be used to argue that field lines are also equipotentials. However, variations in the electron pressure (due to number density differences) can cause an electric field to form along a magnetic field line to balance that pressure gradient. This leads to the concept of “thermalized potential” along a field line:

$$\phi_p = \phi_{p,0} + T_e \ln \left(\frac{n_e}{n_{e,0}} \right), \quad (1)$$

where ϕ_p is the potential along the field line, $\phi_{p,0}$ is the potential on the field line at the channel center, T_e is the electron temperature, n_e is the electron density along the field line, and $n_{e,0}$ is the electron density on the field line at the channel center.

Sputter erosion of the ceramic wall is the primary life-limiting mechanism in modern Hall thrusters. This erosion is caused by ions that bombard the walls at significant energies that come from the accelerating axial electric field as well as the Debye sheath formed at the wall surface. If the magnetic field can be contoured such that electric potentials are high and electron temperatures are low at the wall, this would minimize the bombarding ion energy and subsequent sputter erosion of the wall. The concept of magnetic shielding seeks to utilize the idea that magnetic field lines are isothermal to connect the low-temperature region near the anode to the channel wall near the exit plane (see Fig. 1). Contouring the magnetic field this way has two effects – (1) it reduces the electron temperature near the wall, thereby reducing the ion energy gained in the sheath, and (2) it forces the second term in Eq. (1) to be small, making the magnetic field line near the wall close to an equipotential.

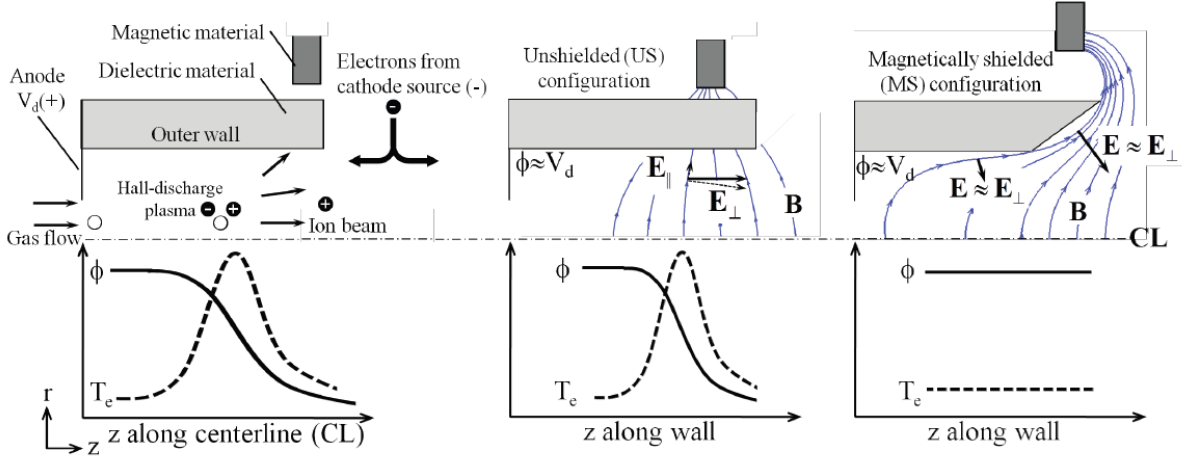


Figure 1. Illustration of the concept of magnetic shielding. By properly shaping the channel wall and contouring the magnetic field, high plasma potentials and low electron temperatures can be maintained in the near-wall region. This significantly reduces ion energies at the wall, mitigating the sputter erosion issue. Image taken from Ref. 8.

In order to determine whether magnetic shielding can be applied to a higher power Hall thruster, the 300M channel wall and magnetic circuit were modified to create the NASA-300MS (hereafter referred to as the 300MS). The 300MS has been thoroughly characterized at the NASA Glenn Research Center (GRC). Details about the design process and how it was guided by simulation, along with performance and thermal characterizations can be found in Ref. 11. A far-field plume efficiency analysis of the 300M and 300MS can be found in Ref. 12. This paper describes the measurements taken within and just downstream of the channels of the 300M and 300MS using a high-speed reciprocating Langmuir probe as well as flush-mounted Langmuir probes. A cylindrical Langmuir probe was used to determine axial profiles of electron temperature and floating potential in the 300M and 300MS. Axial profiles of electron temperature and how they vary with operating condition between the 300M and 300MS can provide important data on the behavior of these thrusters at higher power levels. Flush-mounted Langmuir probes were used at the inner and outer channel walls to measure plasma potential and electron temperature to verify that the 300MS is magnetically shielded. These measurements also provide critical data for the validation of modeling efforts at JPL, which can be essential to determining the overall lifetime of magnetically shielded devices.

The paper is organized as follows: Section II describes the vacuum facility, Hall thrusters, and diagnostics used in this study. Section III provides the results and discusses the trends from the cylindrical Langmuir probe on the 300M and 300MS and the flush-mounted Langmuir probes on the 300MS. Section IV provides concluding remarks and discusses future work.

II. Experimental Apparatus

A. Vacuum Facility

Testing for this study was conducted within Vacuum Facility 5 (VF-5) at NASA GRC. The facility is a 4.6-m-diameter by 18.3-m-long cylindrical chamber that is equipped with cryogenic surfaces as well as 20 0.8-m-diameter oil diffusion pumps. Facility pressure was monitored with an exposed hot-cathode ionization gauge that was mounted near the test article in order to obtain a more accurate measurement of the backpressure the thruster was exposed to during operation. Facility base pressures of 4×10^{-7} Torr were routinely achieved. For a total flow rate of 40 mg/s, the facility pressure was 2.0×10^{-5} Torr, corrected for xenon. Facility pressure did not exceed 2.3×10^{-5} Torr, corrected for xenon, during the course of the test.

B. Hall Thrusters and Support Equipment

The test articles for this study were the 300M and 300MS Hall thrusters. The 300M is a laboratory device whose nominal operating condition is 500 V discharge voltage and 20-kW discharge power. Performance testing of the 300M was completed within VF-5 in 2011.¹ Extensive testing in the near-field and far-field plume has also been performed on the 300M within VF-5 at GRC.^{2,3,12} The 300M can achieve total thrust efficiencies of up to 67% and produce over 1 N of thrust. The 300MS is a retrofitted version of the 300M that has incorporated magnetic shielding in order to demonstrate longer lifetimes on a high power thruster. It includes a new boron nitride discharge channel

with a pre-machined chamfer near the exit plane, as well as magnetic circuit modifications to achieve the shielded configuration. The 300MS has also undergone extensive performance, thermal, and far-field plume testing within VF-5 at GRC.^{11, 12} More information on the 300MS and how the magnetic circuit design was guided by simulation can be found in Ref. 11.

The support equipment for thruster operation was identical between the 300M and 300MS. Xenon was supplied through commercially available mass flow controllers with an accuracy of $\pm 1\%$ of the reading. A commercial power supply capable of outputting 2000 V and 100 A was used to sustain the discharge. Separate power supplies were used to power the magnets, as well as the cathode keeper and heater. The thruster's center-mounted cathode is a laboratory model based on the discharge cathode assembly of NASA's Evolutionary Xenon Thruster (NEXT) and has been used on the NASA-400M, -457Mv1, and -457Mv2 Hall thrusters.^{1, 13} The cathode flow rate was fixed at 8% of the anode flow rate throughout testing. A symmetric magnetic field topology (one that is symmetric about the channel centerline) was used for all operating conditions presented in this study. The field strength was chosen to maximize the anode efficiency as measured by a thrust stand:

$$\eta_a = \frac{T^2}{2\dot{m}_a P_d}, \quad (2)$$

where η_a is the anode efficiency, T is the measured thrust, \dot{m}_a is the anode mass flow rate, and P_d is the discharge power.

C. Internal Diagnostics

The diagnostics used in this study include a cylindrical Langmuir probe as well as flush-mounted Langmuir probes. The cylindrical probe was primarily used to determine the spatial variations in electron temperature within and just downstream of the thruster channel on both the 300M and 300MS. This was facilitated using a high-speed axial reciprocated probe (HARP) system. The flush-mounted Langmuir probes were used to determine the electron temperature and plasma potential near the inner and outer channel walls close to the thruster exit plane. These probes were only utilized on the 300MS, since their intended purpose was to verify that magnetic shielding had been achieved.

Figure 2 shows the general setup used for internal measurements with the cylindrical Langmuir probe. The thruster was placed on a commercially available motion table to allow movement in the radial direction. A leveling table was used to ensure the thruster firing axis was parallel to the centerline of the vacuum facility. The probe was placed on the HARP to allow for rapid injection and retraction in the axial direction. Due to the large acceleration loads generated when the HARP actuates, this stage was rigidly mounted to the vacuum chamber on a stationary platform. This setup, where the HARP remains fixed while the thruster moves, allows for full mapping of the channel while minimizing any shifting of components due to the acceleration loads. When data were not being taken, the thruster was moved sufficiently far away to prevent excessive heating of the HARP and probe due to ion beam impingement.

While data were collected that covered a significant region within the channel, only data taken along channel centerline will be discussed in this paper. Additional details of the HARP and diagnostics can be found in the sections below.

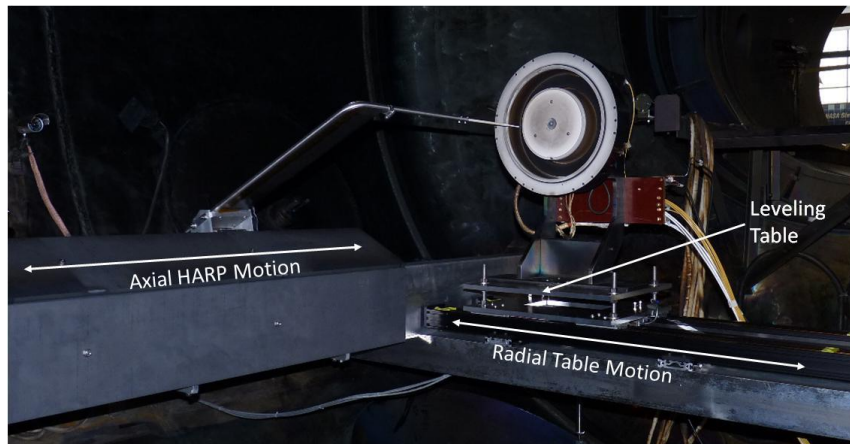


Figure 2. Photograph of the general setup for internal measurements using the cylindrical Langmuir probe. The thruster moves on a radial table while axial motion of the probe is provided by the HARP.

1. HARP

The HARP used in this study is a commercially available, magnetically-actuated motion table capable of speeds up to 1.7 m/s. These speeds are necessary to prevent excessive heating of the probe while it is inside the thruster channel. Due to the large acceleration loads created during actuation, the HARP is rigidly mounted onto a platform attached to the facility. This minimizes any shifting that would occur under loading. The HARP itself is protected from thruster ion impingement with a set of two graphite plates. For this study, the HARP speed was set to 1.5 m/s, resulting in a residence time within the discharge channel of approximately 110 ms.

The probe arm that attaches to the HARP is comprised of a cylindrical stainless steel tube with an outer diameter of 12.7 mm. An additional frame composed of square tubing and sheet metal were attached to the back end of the tube to provide further rigidity and dampen probe tip oscillations due to the acceleration loads. The majority of this structure was covered in flexible graphite sheets to minimize tube heating and backspattered material from beam ion impingement. The probe itself is held in place within the tube using a set of six set screws.

2. Cylindrical Langmuir Probe

The mechanical design of the cylindrical Langmuir probe used in this study closely resembles that of Reid.¹⁴ A 0.255-mm-diameter pure tungsten wire was placed within a 1.6-mm-diameter double-bore alumina tube. This tube was then telescoped within a larger, 6.4-mm-diameter single-bore alumina tube for added durability. The front 75 mm of the double-bore tube was then covered by a boron nitride collar with three steps of increasing thickness (see Fig. 3). This collar was used to increase the survivability of the probe housing when interrogating the plasma at higher discharge powers.¹⁵ The tubes and collar were held together using high-temperature ceramic paste. The final length of the probe tip was approximately 2 mm, providing a length-to-diameter ratio of approximately eight to reduce end effects. The majority of the electrical lines leading from the probe to the measurement circuit were comprised of shielded coaxial cabling.

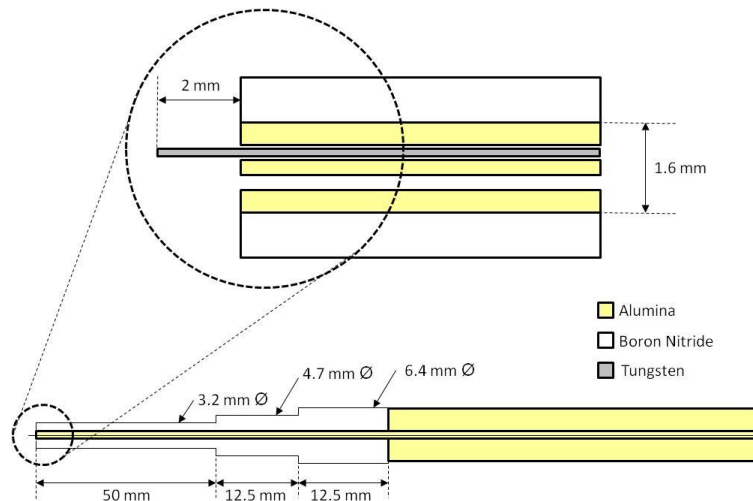


Figure 3. Schematic of the cylindrical Langmuir probe used in this study. Not to scale.

Figure 4 shows the electrical diagram for the circuit used to measure applied voltage and collected current from the cylindrical Langmuir probe in this study. The same circuit was used for the flush-mounted Langmuir probes described in the next section. The probe bias waveform was generated via computer program and sent through the analog-out channel of the data acquisition and control system (DACS). The signal was then amplified using a 1000-V, 40 mA bipolar power supply. A 100- Ω , 25-W power resistor was used to measure the collected current from the probe. The applied voltage was measured using a voltage divider comprised of 10 M Ω and 0.13 M Ω 0.25-W metal film resistors. The current and voltage signals were passed through voltage-following instrumentation and isolation amplifiers before being measured at the DACS. The instrumentation amplifiers were used to minimize the zero drift and amplification noise in the circuit. Blocking diodes were used across the inputs of the instrumentation amplifiers to protect them from large electrical spikes. The probe was biased using a symmetric triangle wave at a frequency of 375 Hz. Data were collected by the 16-bit DACS at a scanning rate of 375 kHz, resulting in approximately 500 points per Langmuir probe I-V characteristic. These values were chosen as a satisfactory compromise between

minimizing probe capacitive current and maximizing spatial resolution of the collected data. The measurement circuit was calibrated before and after testing and displayed excellent linearity and repeatability.

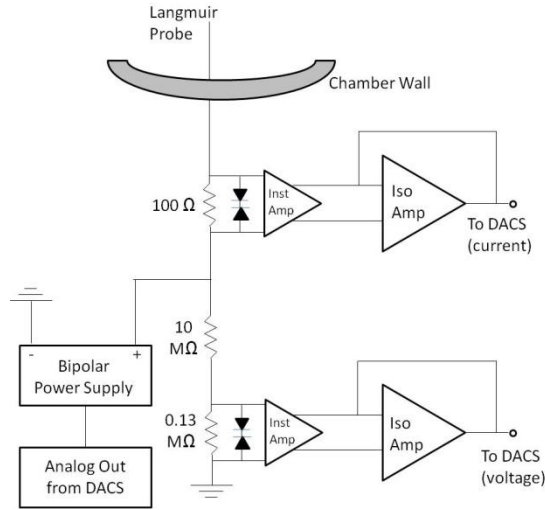


Figure 4. Electrical diagram of the circuit used to measure applied voltage and collected current for the Langmuir probes used in this study.

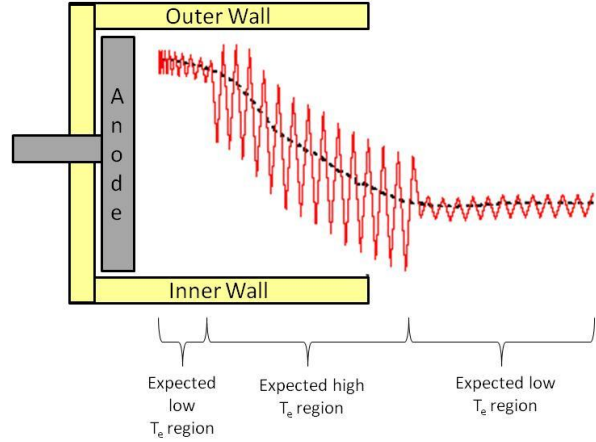


Figure 5. Illustration of how the probe voltage was generated along channel centerline for the cylindrical Langmuir probe. Voltage was applied around the measured floating potential (dotted line), and the amplitude of the voltage was increased in the region of high expected electron temperatures. Not to scale.

Use of software to generate the voltage waveform allowed for more control in how the probe bias was applied as the probe entered the channel. The probe was initially fired into the channel while isolated from ground in order to obtain the floating potential profile along channel centerline. The waveform was then divided into three regions – a near-anode region and near-field plume region where the electron temperature is expected to be low, and an exit-plane region where the electron temperature is expected to be high. Since the range of probe voltages required to properly sample the plasma increases with electron temperature, this allowed for increased probe bias amplitudes limited to the region that requires it (see Fig. 5). The increased amount of control allows for a more complete data set with fewer injections into the channel, increasing data collection rate and probe longevity. However, in order to improve measurement fidelity, five data sets (i.e. probe injections) were obtained at channel centerline. Each data set was analyzed separately and then all sets were averaged to obtain the final axial profiles of plasma properties.

Analysis of the resulting data largely followed simple Langmuir probe theory.^{16, 17} First, the probe floating potential was found by determining the probe voltage at which the collected current is zero. Then, ion current was subtracted from the I-V characteristic and the logarithm of the resulting current was plotted as a function of probe bias. The inverse slope of the region around the floating potential was taken to be the electron temperature in eV. While the ion current was initially assumed to be equal to the collected current at the lowest probe voltage, the electron temperature was iteratively solved for until the assumed ion saturation current and calculated electron temperature formed a consistent solution. Due to variations in line fits for a given I-V characteristic, the uncertainty in the measured electron temperature is taken to be $\pm 20\%$.

The capacitive current in the probe line was characterized by applying a triangle waveform bias to the probe at various amplitudes and frequencies when the thruster was off. The capacitive current was assumed to follow the relation:

$$I_{cap} = -C \frac{dV}{dt}, \quad (3)$$

where I_{cap} is the capacitive current, C is the line capacitance, and dV/dt is the derivative of applied probe voltage with time. Once the line capacitance was determined, it was used with the calculated dV/dt to subtract out the capacitive current in the I-V characteristics prior to any analysis. For all data presented in this paper, capacitance

values were approximately 600 pF. The majority of the line capacitance appeared to come from the coaxial cabling used to connect the probe to the measurement circuit.

3. Flush-mounted Langmuir Probe

Langmuir probes imbedded in the inner and outer channel walls were used to determine the plasma potential and electron temperature in the near-wall region of the 300MS. These measurements were taken to verify that the thruster was magnetically shielded. Based on the discussion in Section I, magnetic shielding was assumed to be achieved if the near-wall plasma potential was close to anode potential and the near-wall electron temperature was low ($\sim 5\text{-}10$ eV). These values should be observed near the thruster exit plane where beam energies and electron temperatures are high in traditional Hall thrusters, resulting in large erosion rates of the channel walls.

Due to the limited space for wiring near the exit plane of the 300MS, only one axial position was interrogated along each channel wall. For the outer wall, the probe was placed $0.034L$ upstream of the exit plane, where L is the thruster channel length. Since more wall material was present near the exit plane along the inner wall, the probe was able to be placed slightly farther downstream, at $0.025L$ upstream of the exit plane. For both walls, an additional probe was included for redundancy at the same axial location but at a different clock position. Also, the magnetic circuit alterations to the 300MS prevented the probe wires from being inserted at an angle to be flush with the chamfered wall surface (see Fig. 6a). To overcome this issue, the wires were inserted in a purely radial fashion and the probe tips were shaped to the correct angle using a diamond file (see Fig. 6b).

The probe tip itself was comprised of 0.51-mm-diameter pure tungsten wire, inserted directly into a hole drilled into the channel wall. Each probe tip was held in place with high-temperature ceramic paste. Probe lead wires were protected with fiberglass insulation until they were sufficiently far away from the thruster plume to avoid significant plasma heating. Wiring for the inner wall probes were routed through the hole in the center of the thruster that houses the cathode, and were covered by the boron nitride plate placed over the inner front magnetic pole. Once sufficiently far away, the remaining length of wire to the measurement circuit was comprised of shielded coaxial cabling. See Fig. 7 for photographs of the flush-mounted probes installed on the 300MS.

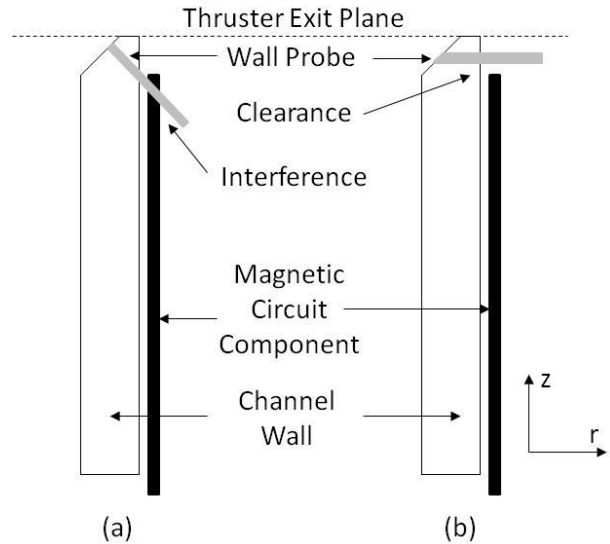


Figure 6. Illustration of how wall probe had to be oriented to avoid interference with adjacent magnetic circuit components.

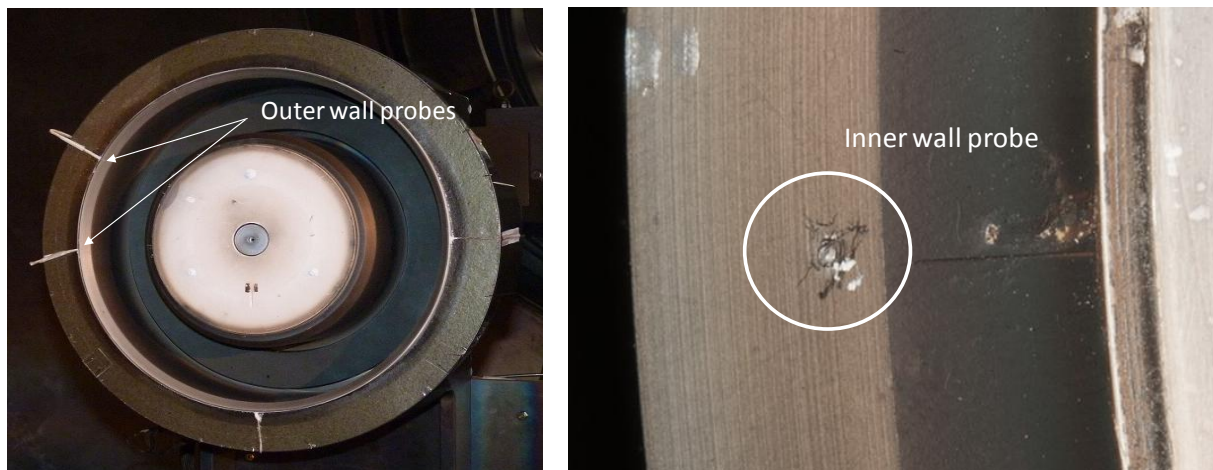


Figure 7. Photographs of flush-mounted Langmuir probes installed on the 300MS. (Left) Probes on the outer wall, with lead wires seen routed around outer front magnetic pole. (Right) Close-up of probe on the inner wall.

The measurement circuit used for the flush-mounted probes was identical to the one used for the cylindrical Langmuir probe. A triangle wave at a frequency of 2 Hz was used to bias each probe. Four I-V characteristics were captured for each wall probe at each operating condition, with each characteristic containing approximately 125,000 points. All I-V characteristics were plotted together and boxcar averaging of 2000-2500 points (equivalent to ~ 0.5 V) was performed. Analysis of the data largely followed simple Langmuir probe theory, similar to the data from the cylindrical Langmuir probe. The plasma potential was found by fitting lines to the transition and electron saturation regions on a semilog plot of electron current. The probe voltage at which these lines intersect is taken as the plasma potential.

At several operating conditions the data from the inner wall probe exhibited signs of leakage current. These I-V characteristics appeared to have been shifted in the positive direction (excess electron current), artificially reducing the measured floating potential. For these data sets, the characteristic was shifted down until the transition region of the characteristic exhibited a high degree of linearity in semilog space. While this technique likely does not fully recover the characteristic with no leakage current, the calculated plasma properties were consistent with properties measured at the outer wall. Results from I-V characteristics that showed signs of leakage current are noted as such in Section III.

III. Results and Discussion

Langmuir probe measurements were taken within the discharge channels of the 300M and 300MS using a high-speed reciprocating stage. Flush-mounted Langmuir probes were also used to verify that the 300MS is magnetically shielded. The results are presented and discussed within this section. Tested operating conditions will be referred to as YYY V, ZZ kW, where YYY is the discharge voltage in volts and ZZ is the discharge power in kW. Axial profiles along channel centerline of the measured floating potential, electron temperature, and calculated plasma potential are presented for the 300M. This is followed by measured electron temperatures and plasma potentials along the inner and outer channel walls of the 300MS. Finally, a preliminary comparison is made between axial profiles of floating potential and electron temperature between the 300M and 300MS. For all axial profiles, data is plotted as distance from the thruster exit plane, with negative values being upstream (within the channel) and positive values being downstream (in the near-field plume).

A. Axial Profiles for the 300M

Figure 8 shows the measured axial profiles of probe floating potentials along channel centerline for the 300M. All floating potentials are reported with respect to facility ground. All profiles exhibit a similar shape, starting at approximately 90% of the discharge voltage and dropping below facility ground in the very-near-field plume ($0.5L$ downstream of the exit plane) before approaching ground potential in the far field plume. The location of maximum (negative) slope was found to be $0.15L - 0.24L$ upstream of the location of the acceleration zone, which is discussed further below. This trend is consistent with prior measurements taken by Reid on a lower-power Hall thruster.¹⁴

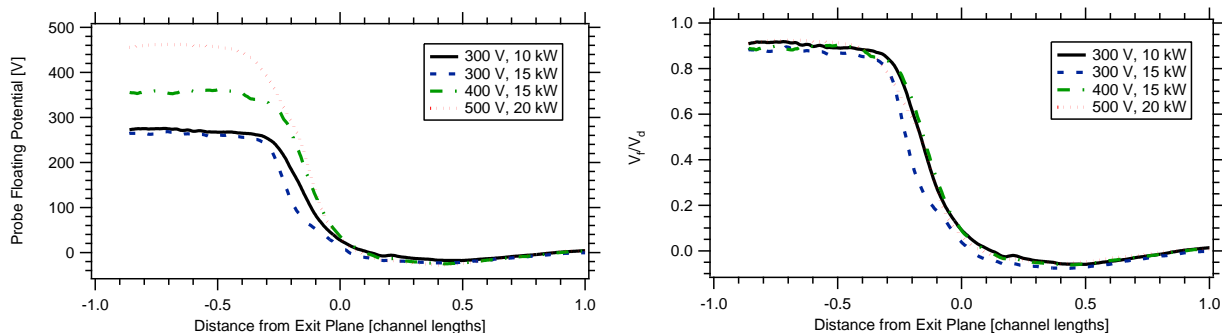


Figure 8. (Left) Measured probe floating potential axial profiles along the channel centerline of the 300M. (Right) Once normalized by the discharge voltage, these profiles were found to be highly similar.

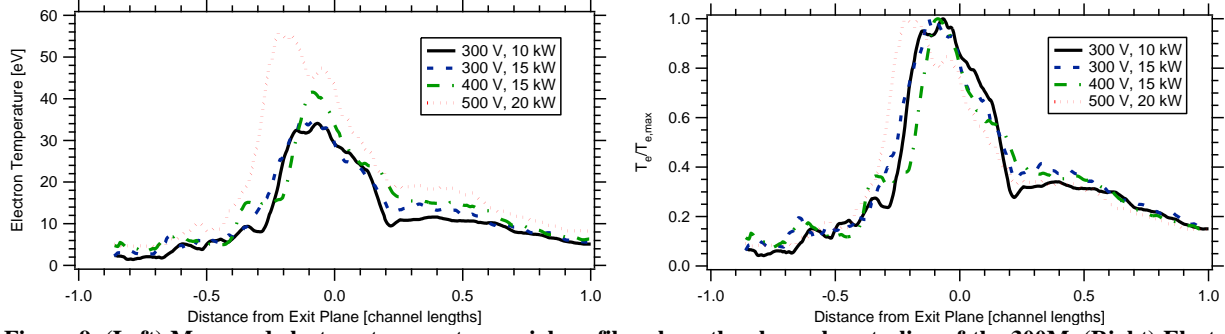


Figure 9. (Left) Measured electron temperature axial profiles along the channel centerline of the 300M. (Right) Electron temperature profiles normalized by the peak temperature. All profiles are highly similar, with only slight shifts in the location of the peak.

Figure 9 shows the measured axial profiles of electron temperature along channel centerline for the 300M. Profiles show the expected trend of elevated temperatures in the vicinity of the thruster exit plane, as well as increased peak temperatures at higher discharge voltages. Table 1 shows these peak temperatures as a function of operating condition, as well as their locations with respect to the thruster exit plane. All peak electron temperatures occurred fairly close to one another with the exception of 500 V, 20 kW. Furthermore, for the other three operating conditions, the peak electron temperature occurred $0.06L - 0.12L$ downstream of the location of maximum (negative) slope of the floating potential. At 500 V, 20 kW, the peak electron temperature occurred upstream of this maximum slope. As will be discussed further below, this is just one reason to believe the measured peak at 500 V, 20 kW has a higher degree of uncertainty. As mentioned in the previous section, five data sets were obtained at channel centerline in an effort to improve measurement fidelity. The peak temperature and location shown for 500 V, 20 kW was measured multiple times, indicating that this point was repeatable.

Table 1. Measured peak electron temperatures for the 300M. Peak locations are given in units of channel length from the thruster exit plane.

Operating Condition	Peak Electron Temperature [eV]	Peak Location [channel lengths]
300 V, 10 kW	34	-0.07
300 V, 15 kW	35	-0.13
400 V, 15 kW	42	-0.09
500 V, 20 kW	56	-0.22

Due to a number of factors, measurement of the local plasma potential using a floating emissive probe^{15, 18-20} proved difficult on the 300M. The larger thruster size is expected to result in longer times in which the probe was subjected to the harsh plasma environment, resulting in a lower probe survival rate. In an effort to still obtain the plasma potential profile along channel centerline, the measured floating potentials and electron temperatures were used to estimate the plasma potential using Eq. (4):

$$\phi_p = V_f + \zeta T_e, \quad (4)$$

where ϕ_p is the plasma potential, V_f is the floating potential, T_e is the electron temperature, and ζ is a proportionality factor. Based on previous internal measurements²¹, an average proportionality factor of 4.6 was used in Eq. (4), which is fairly close to the ideal value of 5.3 for a xenon plasma.¹⁷

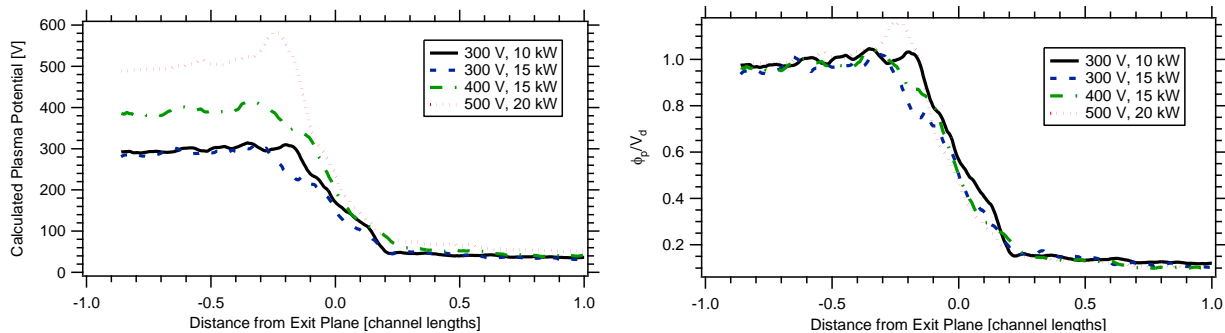


Figure 10. (Left) Calculated plasma potential axial profiles along the channel centerline of the 300M. (Right) Profiles non-dimensionalized by the discharge voltage, showing highly similar acceleration zones.

Table 2. Calculated acceleration zone locations and widths for various operating conditions of the 300M.

Operating Condition	Acceleration Zone Location [channel lengths]	Acceleration Zone Width [channel lengths]
300 V, 10 kW	0.03	0.31
300 V, 15 kW	-0.01	0.42
400 V, 15 kW	0.01	0.42
500 V, 20 kW	0.02	0.31

the acceleration zone width and location appear to be fairly constant across operating conditions. The zone is centered close to the thruster exit plane with a width $\sim 0.3L - 0.4L$, which is fairly consistent with previous measurements on a lower-power thruster.²² The electron temperature peak occurs between the acceleration zone location and the location of maximum (negative) slope of the floating potential, except at 500 V, 20 kW. This trend is useful information for future measurements when estimating the location of the high-temperature region. Figure 10 shows that a slight rise in plasma potential occurs at 500 V, 20 kW around $z = -0.25L$, which is the result of the large peak electron temperature measured around this location. Since this rise in potential is not expected to occur and has not been seen in prior measurements, it is further evidence that the peak electron temperature at 500 V, 20 kW has a higher degree of uncertainty. Figure 11 compares the measured electron temperature profile at 500 V, 20 kW to the profile required to yield a constant plasma potential in the region upstream of the acceleration zone. The predicted profile would yield a slightly lower peak temperature that would occur slightly further downstream.

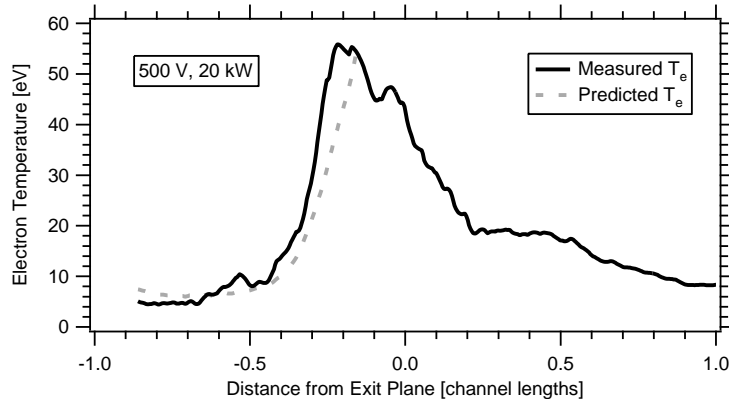


Figure 11. Comparison of measured and predicted axial profiles of electron temperature at 500 V, 20 kW for the 300M. The predicted value is the required electron temperature to yield the expected constant plasma potential upstream of the acceleration zone.

The general uniformity between profiles of electron temperature and plasma potential is somewhat surprising given the range of discharge voltages and powers that were tested. Prior measurements on a lower-power thruster have shown that the acceleration zone (and peak temperature) gets pushed downstream and becomes narrower with increased anode mass flow rate (or equivalently, increased discharge current), while the acceleration zone tends to begin further upstream as the discharge voltage is increased. Furthermore, the peak electron temperature is expected to drop with increased anode mass flow rate.^{14, 15, 22} None of these trends are seen in the data from the 300M. However, the above trends were not observed across all operating conditions on the lower-power thruster. Varying trends were found at off-nominal voltages and flow rates that deviate from the ones outlined above. Furthermore, the tested operating conditions on the 300M did not deviate significantly in discharge voltage or discharge current density from the nominal condition of 500 V, 20 kW. With this in mind, along with the possibility of competing trends in the tested operating conditions, the similarity in profiles may be the result of subtle differences not easily resolved by the Langmuir probe study.

B. Plasma Properties at the Channel Walls of the NASA-300MS

Flush-mounted Langmuir probes were used near the thruster exit plane to verify that magnetic shielding was achieved on the 300MS. Magnetic shielding was assumed to occur if the measured plasma potential was near anode

potential and the measured electron temperature was small (~5-10 eV). Figure 12 shows representative I-V characteristics from the probes at the nominal operating condition of 500 V, 20 kW. Both sets of data exhibit a typical shape for Langmuir probe data. However, the data from the inner wall is clearly shifted up, indicating signs of leakage current. In fact, the floating potential shifted to such a low voltage that it was never measured. Based on the shape alone, the true floating potential is expected to be approximately 470 V. Also, the measured current at the inner wall is significantly less than that measured at the outer wall. This trend was observed at all operating conditions. Since the measured electron temperatures are similar between the inner and outer walls, this trend could indicate that the plasma density is significantly lower along the inner wall compared to the outer wall. Differences in probe collection area between the two walls could also be a factor. Pre-test and post-test observations indicated that the outer wall probe was slightly protruding out from the wall, while the inner wall probe was slightly recessed. This difference would cause the probe collection area to be larger on the outer wall, resulting in higher collected currents. However, the difference in probe area alone cannot account for the large difference observed in collected current.

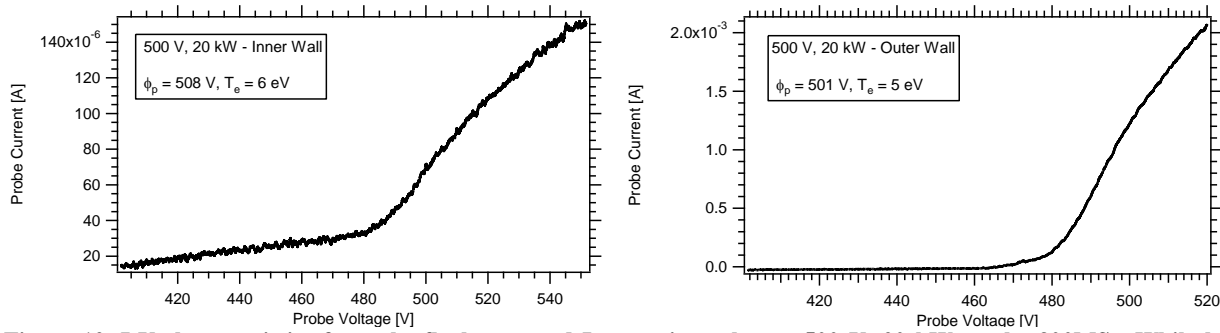


Figure 12. I-V characteristics from the flush-mounted Langmuir probes at 500 V, 20 kW on the 300MS. While both characteristics exhibit a typical shape, the collected current on the inner wall is significantly less than that collected at the outer wall. Signs of leakage current are also exhibited by the data from the inner wall.

Table 3 shows the measured plasma properties at the channel walls near the exit plane of the 300MS. All reported values of plasma potential are referenced with respect to cathode potential. Values with an asterisk denote that they were determined from data that showed signs of leakage current. As can be seen in Table 3, the plasma properties between the inner and outer walls are highly consistent, even when leakage current was observed on the inner wall probe. For all operating conditions, measured plasma potentials are slightly higher than anode potential. This indicates that ions near the wall will have a negligible amount of beam ion energy. For most operating conditions, the measured electron temperatures were around 5 eV. This indicates a small amount of sheath ion energy at the wall as well. However, at 400 V, 20 kW and 600 V, 20 kW, elevated temperatures around 10 eV were observed.

Table 3. Measured plasma potentials and electron temperatures at the inner and outer walls of the 300MS, near the thruster exit plane. All plasma potentials are with respect to cathode potential. Magnetic shielding was achieved at all operating conditions. Values with an asterisk were calculated from data that exhibited signs of leakage current.

Operating Condition	Inner Wall		Outer Wall	
	Plasma Potential [V]	Electron Temperature [eV]	Plasma Potential [V]	Electron Temperature [eV]
300 V, 10 kW	310	4	305	5
300 V, 15 kW	311	6	304	4
400 V, 15 kW	410*	7*	402	5
400 V, 20 kW	413*	11*	408	11
500 V, 20 kW	508*	6*	501	5
600 V, 20 kW	600*	11*	603	12

The reason behind these elevated temperatures is still under investigation. Data from 600 V, 20 kW indicate a higher degree of current oscillation compared to other operating conditions, which may be a reason for the elevated temperatures observed. However, oscillations from 400 V, 20 kW appear comparable to those observed at 500 V, 20 kW. While the thruster appears to not be perfectly magnetically shielded at these conditions, no saturation of the

thruster magnetic circuit was observed. Thus, the magnetic field shape and strength should have been sufficient to provide adequate shielding. Even though these temperatures are higher than expected for a magnetically shielded thruster, they are still likely much lower than what would have been observed in an unshielded configuration. Overall, the measured plasma properties at the walls confirm that magnetic shielding was successfully implemented on the 300MS.

C. Preliminary Comparison between the 300M and 300MS

Internal measurements of the 300MS at channel centerline were found to be more difficult to obtain than on the 300M. This is likely due to the more hostile nature of the plasma at centerline. Since less plasma is in contact with the channel walls, the plasma density is expected to be higher at centerline for a given discharge current density. Furthermore, Hall2De simulations have shown that the peak electron temperature is considerably higher in a magnetically shielded thruster, although this has yet to be verified by experiment.¹⁰ This results in additional plasma heating of the probe at centerline for a magnetically-shielded thruster. In fact, significant probe degradation was observed when taking measurements at 500 V, 20 kW on the 300MS.

For these reasons, only data from 300 V at 10 and 15 kW discharge power will be presented here. Figure 13 compares the probe floating potentials along channel centerline at these conditions between the 300M and 300MS. All floating potentials are reported with respect to facility ground. While little change was observed between the two thrusters at 10 kW, the floating potential profile was pushed significantly downstream for the 300MS at 15 kW. The ionization and acceleration zones are expected to occur further downstream on the 300MS since the peak radial magnetic field also occurs further downstream.¹¹ This trend has also been observed on the magnetically shielded H6 thruster.^{8, 10} Prior measurements on the H6 thruster have shown that the ionization and acceleration zones between operating conditions can shift slightly with little change in the measured probe floating potential.^{14, 15} The present data indicate that the downstream shift seen in the 300MS compared to the 300M is more significant at 300 V, 15 kW.

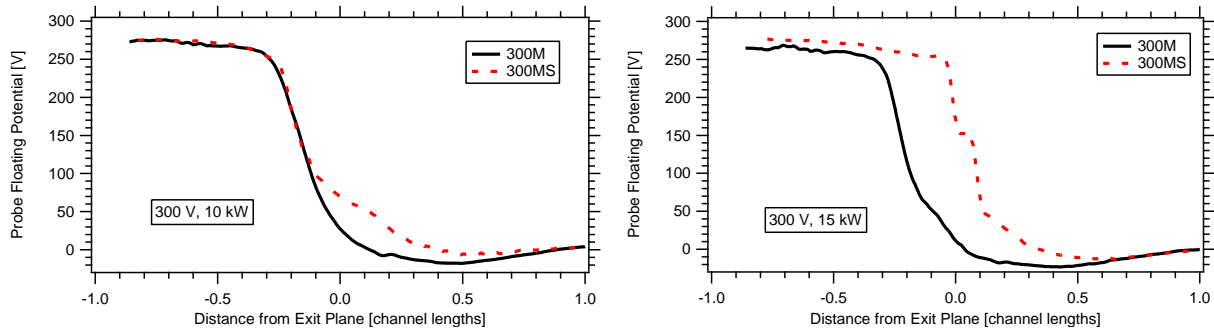


Figure 13. Comparison of probe floating potential axial profiles along centerline between the 300M and 300MS at 300 V, 10 kW (left) and 300 V, 15 kW (right).

Figure 14 compares the measured electron temperature axial profiles along centerline between the 300M and 300MS. As seen in the figure, full profiles could not be obtained for the 300MS configuration. At 300 V, 10 kW, I-V characteristics collected from $z = -0.2L$ to $0.09L$ were deemed too incomplete to determine T_e with reasonable accuracy. Furthermore, at certain locations the floating potential was not properly captured. Attempts to analyze some of these characteristics resulted in values of peak electron temperature approaching 55 eV. If this temperature is correct, it would explain why the probe was not swept in voltage enough to obtain a proper I-V characteristic, since a higher T_e requires a higher voltage sweep in order to capture the same fraction of the I-V characteristic. This large difference in peak temperatures between the 300M and 300MS would also be consistent with simulation results using Hall2De.^{10, 11} An attempt to determine if such a temperature is reasonable is shown in Fig. 15. Equation (4) was used with a plasma potential equal to the discharge voltage, $\zeta=4.6$, and the measured floating potential profile. This gives the electron temperature required to keep calculated plasma potential constant at anode potential, which should be equal to the true electron temperature upstream of the acceleration zone and will be the maximum allowable electron temperature further downstream. Figure 15 shows excellent agreement between this predicted maximum and the measured temperature for $z < -0.2L$. Based on the predicted maximum, 55 eV temperatures do not appear to be consistent with the measured profile, but 40-45 eV maximum temperatures are reasonable if the downstream segment of the measured profile is extrapolated toward the anode. Unfortunately, additional measurements are required to verify the peak temperature in the 300MS at 300 V, 10 kW. The electron

temperature peak can still be inferred to have moved downstream in the MS configuration. As stated before, this is expected due to the shift in peak radial magnetic field for the 300MS.

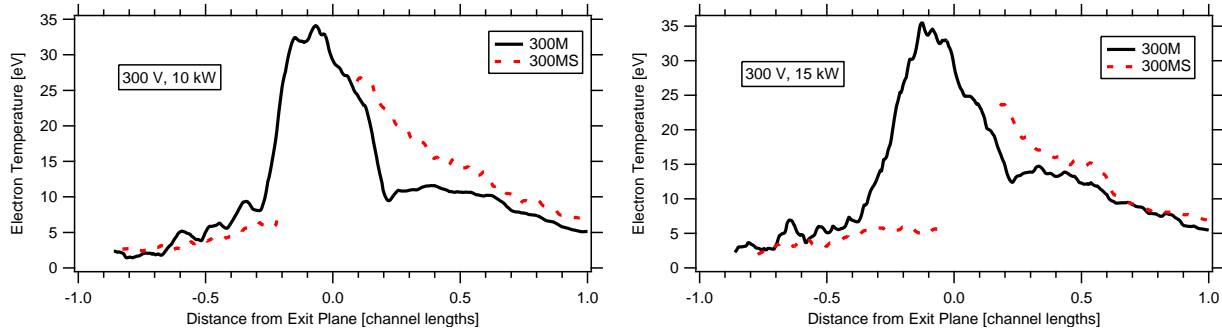


Figure 14. Comparison of electron temperature axial profiles along centerline between the 300M and 300MS at 300 V, 10 kW (left) and 300 V, 15 kW (right). Full profiles could not be obtained for the 300MS.

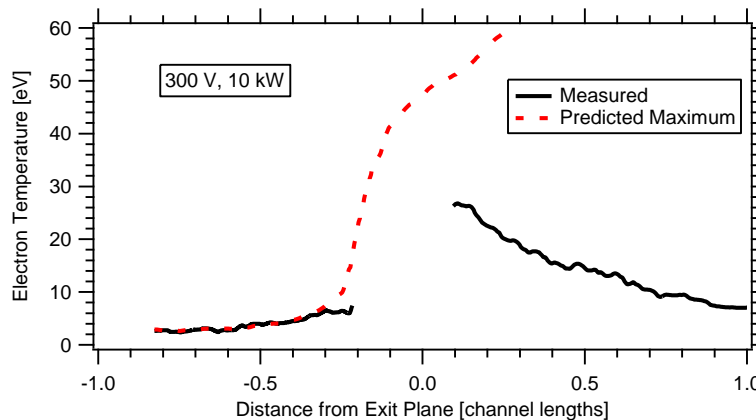


Figure 15. Comparison of measured electron temperature and the predicted maximum electron temperature based on probe floating potential at 300 V, 10 kW for the 300MS.

The reasons for the incomplete temperature profile at 300 V, 15 kW are similar to those for 300 V, 10 kW. However, attempts to analyze I-V characteristics that were deemed too incomplete did not result in significantly higher electron temperatures as they did at 300 V, 10 kW. Furthermore, T_e could not be calculated from $z = -0.02L$ to $0.08L$ because the floating potential was not properly captured in this region (values shown are interpolated between measured points). The reason for this is due to the steep rise in measured floating potential seen in Fig. 13. The cause of this rise is presently unknown, but this region is likely where the primary ionization zone and acceleration zones are. This steep rise is possibly artificial and due to probe overheating, resulting in thermionic electron emission. Such emission would rapidly increase the measured floating potential towards plasma potential. However, probe heating does not appear to be excessive when the probe reaches the anode region since the measured floating potential is still approximately 15 V below anode potential, which is reasonable given the < 5 eV electron temperatures in this region. This steep rise in floating potential was observed at higher discharge voltages and powers as well. As with the 300 V, 10 kW case, the peak electron temperature clearly has been pushed further downstream in the 300MS, as expected. Additional measurements or alternative techniques will be needed to verify the maximum electron temperature in the 300MS.

IV. Conclusions and Future Work

Langmuir probe measurements were taken within the discharge channel of the 20-kW 300M and magnetically-shielded 300MS thrusters to support NASA's Technology Demonstration Mission in the development of a high-power long-life Hall thruster, as well as validate ongoing thruster modeling efforts at JPL using Hall2De. Flush-mounted Langmuir probes within the discharge channel of the 300MS have shown that plasma potentials near anode potential and electron temperatures on the order of 5-10 eV were found near the thruster exit plane, verifying that magnetic shielding has been achieved. Axial profiles along channel centerline of the 300M show calculated acceleration zones centered around the thruster exit plane, with a width of approximately 0.3-0.4 channel lengths.

Peak electron temperatures were found to occur just upstream of the exit plane, with values increasing with discharge voltage as expected. The axial profiles of electron temperature in the 300MS show that the ionization and acceleration zones have moved downstream compared to the 300M as expected. However, measurement of the peak electron temperature was found to be more difficult on the 300MS, and additional measurements or alternative techniques will need to be used to obtain this data.

Data taken within the channel for the 300MS, especially at higher power levels, will have to be analyzed more carefully to determine if additional information can be obtained. This will be important going forward to improve data collection and analysis of future studies on magnetically shielded thrusters. Obtaining such measurements may prove difficult on higher-power thrusters, necessitating alternative plasma diagnostics techniques such as laser-induced fluorescence (LIF) or relying more heavily on flush-mounted Langmuir probes. Lastly, model validation will become critical during the development of future magnetically-shielded thrusters to determine overall service lifetime.

Acknowledgments

The authors would like to thank and acknowledge the Space Technology Mission Directorate for funding this work as well as Timothy Smith for serving as the Project Manager. The authors would also like to thank Kevin Blake, Tom Ralys, George Jacynycz, and George Readus for helping to install the motion system used in this study, as well as maintaining and operating the vacuum facility. Lastly, the authors would like to thank Brian Lee for helping to develop the program that operates and interfaces with the HARP used in this study.

References

- ¹Kamhawi, H., Haag, T. W., Jacobson, D. T. and Manzella, D. H., "Performance Evaluation of the NASA-300M 20 kW Hall Effect Thruster," *47th AIAA/ASME/SAE/ASEE Joint Propulsion Conference and Exhibit*, AIAA-2011-5521, San Diego, CA, July 31 - August 3, 2011.
- ²Herman, D. A., Shastry, R., Huang, W., Soulas, G. C. and Kamhawi, H., "Plasma Potential and Langmuir Probe Measurements in the Near-field Plume of the NASA-300M Hall Thruster," *48th AIAA/ASME/SAE/ASEE Joint Propulsion Conference and Exhibit*, AIAA-2012-4115, Atlanta, GA, July 29 - August 1, 2012.
- ³Huang, W., Shastry, R., Herman, D. A., Soulas, G. C. and Kamhawi, H., "Ion Current Density Study of the NASA-300M and NASA-457Mv2 Hall Thrusters," *48th AIAA/ASME/SAE/ASEE Joint Propulsion Conference and Exhibit*, AIAA-2012-3870, Atlanta, GA, July 29 - August 1, 2012.
- ⁴Shastry, R., Huang, W., Herman, D. A., Soulas, G. C. and Kamhawi, H., "Plasma Potential and Langmuir Probe Measurements in the Near-field Plume of the NASA-457Mv2 Hall Thruster," *48th AIAA/ASME/SAE/ASEE Joint Propulsion Conference and Exhibit*, AIAA-2012-4196, Atlanta, GA, July 29 - August 1, 2012.
- ⁵Soulas, G. C., Haag, T. W., Herman, D. A., Huang, W., Kamhawi, H., Shastry, R., et al., "Performance Test Results of the NASA-457M v2 Hall Thruster," *48th AIAA/ASME/SAE/ASEE Joint Propulsion Conference and Exhibit*, AIAA-2012-3940, Atlanta, GA, July 29 - August 1, 2012.
- ⁶Mikellides, I. G., Katz, I., Kamhawi, H. and Vannoord, J. L., "Numerical Simulations of a 20-kW Class Hall Thruster Using the Magnetic-Field-Aligned-Mesh Code Hall2De," *32nd International Electric Propulsion Conference*, IEPC-2011-244, Wiesbaden, Germany, September 11-15, 2011.
- ⁷Mikellides, I. G., Katz, I., Hofer, R. R., Goebel, D. M., de Grys, K. and Mathers, A., "Magnetic Shielding of the Acceleration Channel Walls in a Long-Life Hall Thruster," *46th AIAA/ASME/SAE/ASEE Joint Propulsion Conference and Exhibit*, AIAA-2010-6942, Nashville, TN, July 25 - 28, 2010.
- ⁸Hofer, R. R., Goebel, D. M., Mikellides, I. G. and Katz, I., "Design of a Laboratory Hall Thruster with Magnetically Shielded Channel Walls, Phase II: Experiments," *48th AIAA/ASME/SAE/ASEE Joint Propulsion Conference and Exhibit*, AIAA-2012-3788, Atlanta, Georgia, July 30 - August 1, 2012.
- ⁹Mikellides, I. G., Katz, I. and Hofer, R. R., "Design of a Laboratory Hall Thruster with Magnetically Shielded Channel Walls, Phase I: Numerical Simulations," *47th AIAA/ASME/SAE/ASEE Joint Propulsion Conference and Exhibit*, AIAA-2011-5809, San Diego, CA, July 31 - August 3, 2011.
- ¹⁰Mikellides, I. G., Katz, I., Hofer, R. R. and Goebel, D. M., "Design of a Laboratory Hall Thruster with Magnetically Shielded Channel Walls, Phase III: Comparison of Theory with Experiment," *48th AIAA/ASME/SAE/ASEE Joint Propulsion Conference and Exhibit*, AIAA-2012-3789, Atlanta, GA, July 30 - August 1, 2012.
- ¹¹Kamhawi, H., Huang, W., Haag, T. W., Soulas, G. C., Shastry, R., Smith, T., et al., "Performance and Thermal Characterization Tests of the NASA-300MS 20 kW Hall Effect Thruster," *33rd International Electric Propulsion Conference*, IEPC-2013-444, Washington, D.C., October 6-10, 2013.
- ¹²Huang, W., Shastry, R., Soulas, G. C. and Kamhawi, H., "Farfield Plume Measurement and Analysis on the NASA-300M and NASA-300MS," *33rd International Electric Propulsion Conference*, IEPC-2013-057, Washington, DC, October 6-10, 2013.
- ¹³Jacobson, D. T., Manzella, D. H., Hofer, R. R. and Peterson, P. Y., "NASA's 2004 Hall Thruster Program," *40th AIAA/ASME/SAE/ASEE Joint Propulsion Conference and Exhibit*, AIAA-2004-3600, Fort Lauderdale, Florida, July 11-14, 2004.

- ¹⁴Reid, B. M. and Gallimore, A. D., "Langmuir Probe Measurements in the Discharge Channel of a 6-kW Hall Thruster," *44th AIAA/ASME/SAE/ASEE Joint Propulsion Conference and Exhibit*, AIAA-2008-4920, Hartford, CT, July 21 - 23, 2008.
- ¹⁵Reid, B. M. and Gallimore, A. D., "Plasma Potential Measurements in the Discharge Channel of a 6-kW Hall Thruster," *44th AIAA/ASME/SAE/ASEE Joint Propulsion Conference and Exhibit*, AIAA-2008-5185, Hartford, CT, July 21 - 23, 2008.
- ¹⁶Hershkowitz, N., *Plasma Diagnostics: Discharge Parameters and Chemistry*, Academic Press, Inc., 1989, Chaps. 3.
- ¹⁷Lieberman, M. A. and Lichtenberg, A. J., *Principles of Plasma Discharges and Materials Processing*, John Wiley & Sons, Inc., Hoboken, NJ, 2005, pp. 185-203.
- ¹⁸Haas, J. M., "Low-Perturbation Interrogation of the Internal and Near-Field Plasma Structure of a Hall Thruster Using a High-Speed Probe Positioning System," Ph.D. Dissertation, Aerospace Engineering, University of Michigan, Ann Arbor, MI, 2001.
- ¹⁹Hershkowitz, N. and Cho, M. H., "Measurement of plasma potential using collecting and emitting probes," *The Journal of Vacuum Science and Technology A*, Vol. 6, No. 3, 1988, pp. 2054-2059.
- ²⁰Linnell, J. A., "An Evaluation of Krypton Propellant in Hall Thrusters," Ph.D. Dissertation, Aerospace Engineering, University of Michigan, Ann Arbor, MI, 2007.
- ²¹Shastry, R., "Experimental Characterization of the Near-Wall Region in Hall Thrusters and its Implications on Performance and Lifetime," Ph.D. Dissertation, Aerospace Engineering, The University of Michigan, Ann Arbor, 2011.
- ²²Huang, W., Drenkow, B. and Gallimore, A. D., "Laser-Induced Fluorescence of Singly-Charged Xenon inside a 6-kW Hall Thruster," *45th AIAA/ASME/SAE/ASEE Joint Propulsion Conference and Exhibit*, AIAA-2009-5355, Denver, CO, August 2 - 5, 2009.